Convention Special Issue – 2020

J. Indian Chem. Soc.,
Vol. 97, No. 12a, December 2020, pp. 2657-2665

Influence of hydrogen on RF-magnetron sputtered ITO films and post hydrogen plasma treatment

Himadri Sekhar Das*[a,b], Rajesh Das[b], Gourisankar Roymahapatra[b], Subir Kumar Maity[c] and Prasanta Kumar Nandi[a]

[a]Indian Institute of Engineering Science and Technology (IIEST), Shibpur, Howrah-711 103, West Bengal, India

[b]Haldia Institute of Technology, Haldia-721 657, West Bengal, India

[c]School of Electronics Engineering, Kalinga Institute Industrial Technology (KIIT), Bhubaneswar-751 024, Odisha, India

E-mail: himadrisekhar_das@rediffmail.com

Manuscript received online 11 November 2020, revised and accepted 22 December 2020

Transparent conducting ITO thin films were prepared by RF-magnetron sputtering using Ar+H_2 environment with different hydrogen dilution at 300ºC and effect of post hydrogen plasma treatment has been investigated. Significant variation on electrical resistivity, mobility, carrier density, optical band gap, refractive index along with the structural diversity and morphology are observed with the variation of hydrogen dilution during deposition. The lowest electrical resistivity and sheet resistance of Ar+H_2 deposited ITO films is 3.12×10^{-4} Ω-cm and 5 Ω/cm respectively and electrical resistivity starts to deteriorate above moderate H_2 dilution. All ITO films show 90% optical transmittance in visible region but drastic fall of visible optical transmittance are noticed for hydrogen plasma exposed ITO films. XRD analysis shows the existence of (222) and (400) major peaks for all as-deposited ITO films and highly dominated (400) peak is observed for high hydrogen diluted ITO film. The existence of high intensity (400) peak is due to increase of indium content in ITO matrix. Significant variations of surface morphology are observed in as-deposited and hydrogen plasma treated ITO films. Low hydrogen dilution shows noticeable improvement of electrical, optical and morphological characteristics. H_2 ambient has an important role in nano-grain formation and hydrogen plasma treatment has a big role for surface modification, grain size reduction as well as in deterioration of electrical and optical properties of ITO films.

Keywords: H_2 ambient, ITO nano-crystallites, surface topography, H-plasma treatment, Haze factor.

1. Introduction

Transparent conducting Indium Tin Oxide (ITO) thin film is an unique material having multifunctional properties and has wide applications in various optoelectronic devices mainly in flat-panel displays (FPDs), organic light-emitting diodes (OLEDs), energy conserving architectural windows, heat reflecting coatings and solar cells due to its unique properties of low electrical resistivity (10^{-5} Ω-cm) and high optical transmission in the visible spectrum and near-IR region for its wide band gap (E_g ~3.9 eV)[1–9]. ITO thin film acts as window layer to visible and NIR region of the solar spectrum due to its high refractive index (μ ~2) and makes rectifying contact as plasmonic metametrial.

ITO films can be prepared by various deposition techniques such as reactive evaporation, pulsed laser deposition, DC and RF- magnetron sputtering, electron beam evaporation, plasma CVD process, spray pyrolysis etc. In the crystalline state, ITO is doped to degeneracy by substitutional tetravalent Sn positioned on trivalent "In" sites, and by the presence of doubly charged oxygen vacancies. In the amorphous state, the carrier sources are less clear, however, there is evidence to suggest that Sn is not efficiently activated and that carriers are contributed primarily by vacancy-like oxygen defects in the amorphous structure[10,11]. Thus, gas phase oxygen content during deposition should be carefully controlled to provide ITO films with optimum electronic proper-

ties in the amorphous and/or crystalline state. A number of researchers have deposited the ITO film using Ar and $Ar+O_2$ ambients. Rottmann and Heckner used pure H_2O vapor and O_2 as reactive agent in sputtering atmospheres and compared the electrical and structural properties of ITO films deposited by reactive DC sputtering[12]. In other study the effect of O_2 concentration in the sputtering ambient on the structure and properties of ITO films was studied[13]. A gradual change from (110) to (311) texture was observed showing improved crystallinity while Itoyama *et al.*, obtained an amorphous like X-ray diffraction pattern for as-deposited magnetron sputtered ITO films[14].

In this paper the effect of different dilution of hydrogen improve the electrical, structural and morphological properties of ITO films has been studied. Role of H_2 in controlling the internal textures as well as morphological changes are discussed. Effect of post hydrogen plasma treatment on electrical, optical, structural and morphological properties of ITO films is also reported.

2. Experimental

ITO thin films were deposited by dual-target RF-magnetron (powered at 13.56 MHz radio frequency) sputtering system (Hind High Vacuum Co. (P.) Ltd.) on glass substrate at substrate temperature T_s = 300°C under reactive environment with $Ar+H_2$ as sputtering gas. Sintered ceramic disc of ITO (Indium Oxide (90%) and Tin Oxide (10%) by weight) with a purity of (99.99%) having 2 inch diameter and 5 mm thickness were used as sputtering target. The sputtering system is made of stainless steel chamber with water cooled capacitive coupled magnetron. Target material is mounted in upper holder and substrate is mounted in lower holder that has controlled rotation facility. The process chamber is evacuated up to a base vacuum of 2.6×10^{-6} torr. The RF-power was varied from 50–100 watt with a step increment of 20 watt. Target to substrate distance was kept at 6 cm for all experiments. Pre-sputtering of ITO target is done in pure argon plasma atmosphere for about ten minutes in order to remove the surface oxide layer of the target before deposition of the film and the glass substrates were also plasma cleaned. The modified chamber design is helpful for uniform ITO thin film growth with high deposition rate and good adhesion with the substrate material. ITO film were deposited with 2%, 6%, and 8% hydrogen dilution [$C_H = (H_2/(Ar+H_2))\times100\%$] in $Ar+H_2$ gas mixture.

The electrical properties of ITO thin films were studied by 4-probe van-der-Pauw technique attached with Hall measurement (Ecopia-HMS-3000) set-up. Optical transmittance and absorbance data of ZnO thin films was measured using microprocessor controlled dual beam UV-Vis (Perkin-Elmer Lamda-35) spectrophotometer (Integrating sphere attached). For absorption measurements in the UV and optical region, the films were coated onto quartz substrates. The refractive indices of ITO films were measured by Spectroscopic Ellipsometry (J. A. Woollam Co.) in the spectral range 193 – 1690 nm.

Structural characterization of ITO films was carried out by crystallographic phase analysis X-ray diffraction (XRD) (Philips PW 1710 diffractometer) (Cu K_α, λ = 1.54178 Å, 2θ scan mode) and High-resolution transmission electron microscopy (HRTEM) (Hitachi Model - HT7700, 120 kV) techniques. The surface morphology was performed by Scanning Electron Microscopy (SEM) (Carl Zeiss SMT Supra 55). Elemental analysis was estimated by Energy dispersive X-ray spectroscopy (EDX) attached with SEM. Surface topography of ITO films was studied by Atomic Force Microscopy (AFM) (Tap 300 G).

3. Results and discussion

The ITO films were deposited under $Ar+H_2$ gas ambient at different C_H values keeping RF-power, chamber pressure fixed at 80 watt, 5 mT respectively at substrate temperature (T_s) 300°C. It was observed that the deposition rate at low hydrogen dilution (C_H = 2%) is 13 nm/min and it decreases with increase of C_H value upto 6 nm/min. H_2 introduction in Ar atmosphere, sputtering ambient becomes diluted. Under pure Argon plasma momentum transfer is maximum, but as hydrogen atoms are lighter than Ar, with introduction of hydrogen the Argon plasma effectively becomes diluted. Moreover the plasma becomes reactive in nature. So, momentum transfer is less and deposition rate decreases. With slight introduction of hydrogen in Ar initial resistivity of ITO films was 5.8×10^{-4} Ω-cm and the lowest resistivity of ITO films were 3.12×10^{-4} Ω-cm under the optimum hydrogen dilution (C_H = 6%). But further increase in C_H values shows the increase in resistivity and it becomes 4.3×10^{-3} Ω-cm for C_H = 8%.

Table 1. Comparative results of electrical and optical properties

Sample (ITO) C_H values	Carrier concentration (cm^{-3})	Mobility (μ) (cm^2/V.s)	Resistivity (ρ) (Ω -cm)	% Transmittance	Haze factor	Sheet resistance R_{sh} = (ρ/t) ohm/square	Figure of merit $\phi^{TC} = T^{10}/R_{sh}$
2%	3.01×10^{20}	3.57	5.80×10^{-4}	~88	30	15.2	1.8×10^{18}
6%	2.73×10^{21}	11.55	3.12×10^{-4}	~87	25	5.2	4.7×10^{18}
8%	9.01×10^{20}	4.92	5.50×10^{-3}	~90	23	57.5	6.0×10^{17}
H-plasma exposed	5.89×10^{20}	1.10	4.37×10^{-2}	~55	20	235	1.1×10^{15}

Table 1 shows the summarized data of resistivity, optical transmittance and figure of merit of as-deposited and H-plasma exposed ITO films. Under Ar+H_2 ambient during ITO deposition, hydrogen act as reducing agent and create oxygen vacancies in ITO film matrix. With C_H = 6% maximum number of free carriers are generated with highest carrier mobility and hence shows minimum resistivity. Physical structure and carrier generation of ITO have been clearly discussed by Tania Konry, Robert S. Marks[15]. Substitution of tin in In_2O_3 bix-bite structure and oxygen vacancies contribute to the high conductivity in ITO film and the material can be represented as $In_{2-x}Sn_xO_{3-2x}$[16]. Further increase of hydrogen dilution during deposition and hydrogen plasma treatment increases free carrier scattering, as a whole carrier mobility decreases and film becomes more resistive.

It is clear from Table 1 as the hydrogen concentration increases in vacuum chamber during deposition time Haze factor of the ITO thin film initially decreases and finally saturates. With the increasing of the hydrogen dilution deposition rate was decreases also diffused transmittance decreases[17–19]. Haze factor was calculated from the ratio of the diffused transmittance and total transmittance. As the hydrogen dilution increases lower the grain size as a result diffused transmittance decreases and finally a sharp decreases of Haze factor of Ar+H_2 deposited ITO films are observed. Excess increase of hydrogen dilution in sputtering gas ambient may cause for increase of amorphous region and void as a result absorption increases in longer wavelength region. Details of scattering mechanism of TCO surface and Haze factor has been discussed by Jager and Zeman[20]. Under high dilution of hydrogen ITO film surface are etched and the surface morphology consists of large number of pores.

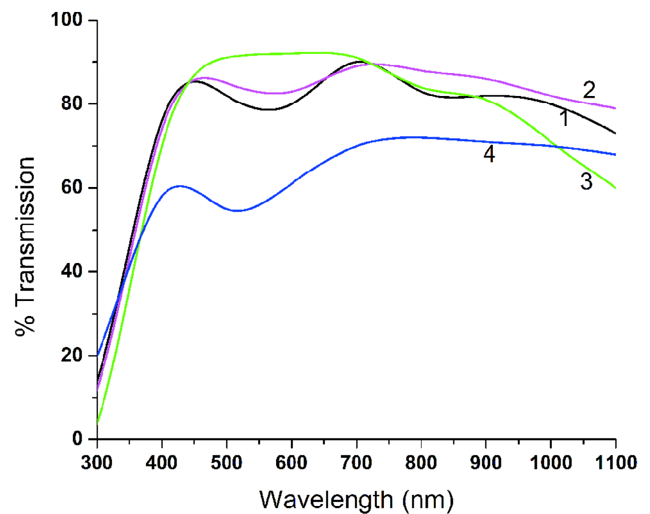

Fig. 1. Optical transmission spectra of RF-sputtered as-deposited and H-plasma exposed ITO thin film: (1) 2%, (2) 6%, (3) 8% and (4) H-plasma exposed.

Fig. 1 shows the optical transmittance spectra of as-deposited and hydrogen plasma treated ITO films. All ITO films were almost around 820 nm thick and show 90% average visible transmittance and almost similar pattern were observed though C_H values were changed from 2 to 6%. But ITO film deposited with C_H = 8% shows more that 90% peak transmittance at 500 nm wavelength and higher absorption value at 1100 nm. On the other hand, drastic change in optical transparency was observed in hydrogen plasma treated ITO film under the following conditions: 60 watt RF-power, H_2 flow 30 sccm, 300°C substrate temperature for 2 min. Optical transmittance becomes less than 60% at 500–700 nm range. Band gap of ITO films were calculated by plotting α^2 vs hν and taking intercepts of the slope and it varies from 4.08 to 4.25 eV. It is important to notice that the refractive index varies with stoichiometry. The variation of band gap and refractive index is shown in Fig. 1 (Inset).

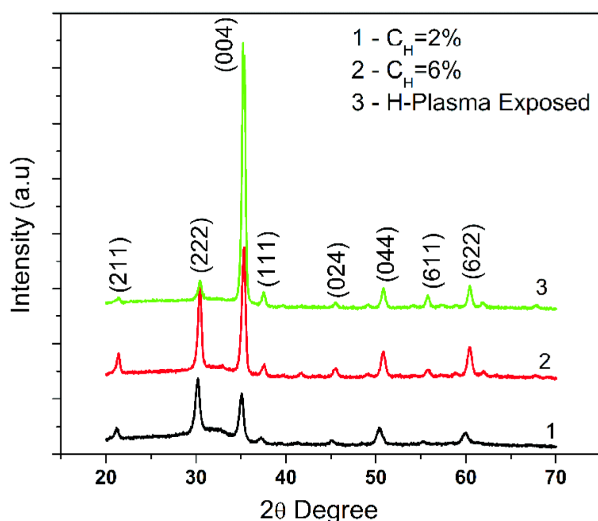

Fig. 2. X-Ray diffraction pattern of ITO films deposited under Ar+H_2 ambient with C_H values: (1) 2%, (2) 6% and (3) H-plasma exposed.

Fig. 2 shows the XRD patterns of the three ITO films deposited using different argon and hydrogen mixture ratios. All the peaks were indexed according to the ASTM powder data[21]. Curve-1, 2 and 3 represent high polycrystalline nature of ITO films deposited with C_H = 2%, 6% and 8% respectively with (211), (222), (400), (111), (024), (044), (611) and (622) crystalline planes of In_2O_3. Here the existences of sharp (222) phase in the ITO thin film corresponds to the cubic bixbyite structure of In_2O_3. In Curve-1, the relatively high intensity of two sharp lines suggests that ITO has preferred orientations with the (222) and (400) planes parallel to the substrate. The existence of small broad peaks with less intensity corresponds to crystallographic defects and amorphization processes that occur mainly in the large In_2O_3 and SnO_2 grains. These crystallographic defects, caused by displacement of In/Sn/O atoms, corroborates with the slight broadening and intensity reduction of the other remaining peaks (Fig. 1).

Curve-2 in the XRD pattern of ITO film deposited with C_H = 6%, (222) and (400) the most intense peaks and (211), (044), (622) peaks with moderate intensity have further intensified. This corresponds to the improvement of crystallinity, which corroborates with the microstructure shown in the HRTEM figure (Fig. 3b) discussed later. Increase of the (400) peak means that film's compactness has deteriorated and the number of inter grain voids/defects has increased (in Table 2 elemental composition variation with hydrogen dilution in ITO film matrix are enlisted). The major common In_2O_3 (222) peak is also intensified which explains the results in well-crystallized ITO structure at higher hydrogen concentration. The other few peaks of In_2O_3 with a few other phases such as SnO_2, SnO (II) and Sn (II) indicate a poor orientation of the film. It is evident that the existence of other broad lines such as (611) of In_2O_3 and (024) for SnO_2 and SnO phases correspond the crystallographic defect and voided region. Because indium and tin have nearly identical masses, the nature of the created defects in In_2O_3 and SnO_2 crystallites should be nearly identical according to the so called cascade phenomenon during the deposition process under hydrogen plasma atmosphere. It is assumed that the effect of H^+ ions during deposition on the spatial locations of Sn^- and In^- sites should be similar. Moreover, without taking into account the peak located at the beginning of the spectrum that we have discussed above, there is no appreciable difference in the angular position of the corresponding peaks for the ITO thin films.

Curve-3 represents the XRD spectrum of hydrogen plasma exposed ITO film and here the (400) peak intensified drastically relative to the other peaks. We can speculate from these results that the driving forces for (400) preferred orientation at high hydrogen concentration ratio is more oxygen

Table 2. Summary of elemental analysis of Indium Tin Oxide (ITO) films

ITO films deposited	Elements				Elemental ratio		Optical bandgap	Refractive
with (Ar+H_2) ambient	O K	In L	Sn L	Total	O/In	In/Sn	(eV)	index
C_H = 2%	70.54	27.07	2.39	100	2.61	11.33	4.14	1.831
C_H = 6%	69.74	27.88	2.38		2.50	11.71	4.25	1.812
C_H = 8%	69.54	28.05	2.41		2.48	11.63	4.08	1.815
H-Plasma exposed	69.27	28.19	2.54		2.46	11.10	–	1.802

Table 3. Crystallite size of ITO film before and after hydrogen plasma exposure

ITO Films	XRD Peak		2θ in degree		β in degree		Crystallite size (nm)		Remarks
	Before	After	Before	After	Before	After	Before	After	
As deposited	(211)	(211)	21.40	21.34	0.43	0.42	18	19.33	Crystallization
(C_H = 6%)	(222)	(222)	30.50	30.42	0.47	0.47	17.53	17.53	along (004) is
and	(004)	(004)	35.30	35.31	0.41	0.43	20.5	19.41	enhanced and
H-Plasma	(044)	(044)	50.80	50.85	0.50	0.47	17.64	18.71	overall crystallite
exposed	(622)	(622)	60.40	60.43	0.51	0.48	18.02	19.32	size is increased

vacancies and their subsequent diffusion in the ITO film at higher temperature. Therefore crystalline ITO deposited at high temperature typically grows (400) preferentially to accommodate the oxygen vacancies on these planes. It is also observed that SnO_2 and SnO phases were detected, implies that tin substitute's indium in the BCC lattice which may cause for the increase of resistivity in ITO film.

The average crystallite sizes 's' have been calculated from different XRD peaks as deposited at C_H = 6% and hydrogen plasma exposed films (shown in Table 3) using Scherrer's formula given by s = $k\lambda/\beta \cos(\theta)$, where 2θ is the angular peak position, λ is the wavelength of the X-rays used and k is a constant which has a value of 0.89 for an assumed spherical grain structure, β is full width half maxima (FWHM) of a selected peak. The degree of film texture was estimated as a ratio *I*(400)/*I*(222) of the most intensive peaks in the XRD patterns of ITO films[22]. It is clear from XRD spectra that the degree of texture increases from 0.9 to 9.5 for ITO films with increases of C_H value during deposition. Average crystallite size is 154 Å for ITO film deposited under Ar+H_2 ambient for C_H = 2%, crystallite size increases to 174 Å when the film is deposited with C_H = 6%. With further increase of C_H, crystallite size increases to 220 Å. As the growth is slower in case of film deposited under higher C_H, crystallite sizes increases. Moreover the single orientation of crystallites along (400) may be due to the slow growth rate at high C_H. For this reason

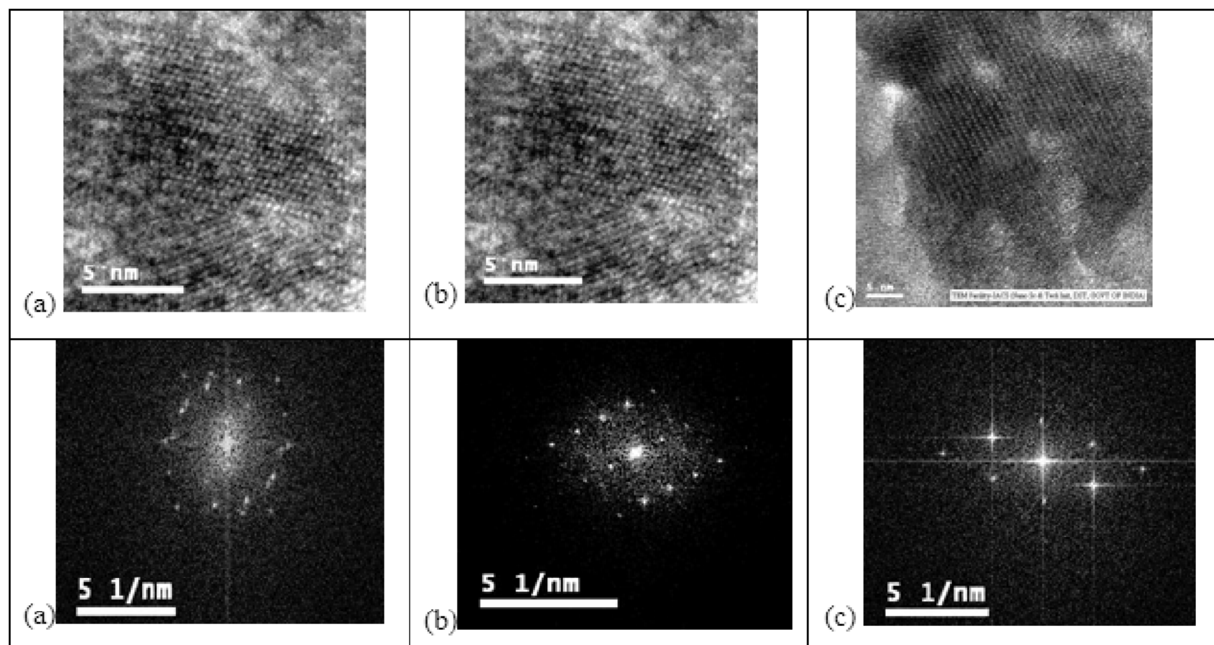

Fig. 3. High resolution transmission electron micrographs (HRTEM) and corresponding First Fourier Transform of ITO films deposited under Ar+H_2 ambient with C_H values: (a) 2%, (b) 6% and (c) 8% of H_2 with Ar.

ITO film deposited with C_H = 2%, 6% random distribution of the microcrystals but for hydrogen plasma exposed the ITO film is highly oriented along (400). Another important observation is that the existence of (400) crystalline peak corresponds to oxygen deficiency.

Fig. 3a, b and c show the transmission electron micrographs and corresponding First Fourier Transform (FFT) of ITO film deposited under different hydrogen concentration ratios. Generally, the sputtered ITO films have a polycrystalline structure. High-resolution transmission electron micrographs (HRTEM images) indicate that most of the sputtered ITO films consist of nanocrystallites. Fig. 3a shows HRTEM and corresponding FFT pattern of ITO films deposited with C_H = 2%. The first Fourier transform (FFT) pattern shown in the Fig. 3a indicates the existence of highly crystalline orientation within the sample. The HRTEM image of the ITO film deposited with C_H = 6% shown in Fig. 3b revealed the crystalline structure having multiple orientations and the dots of the FFT pattern indicates polycrystalline nature of the films. In case of ITO film deposited with C_H = 8%, the HRTEM image shown in Fig. 3c reveals single preferred (400) orientation which corroborates with the X-ray diffraction spectra in Fig. 1c. The existence of the dots in FFT pattern corresponds to the high degree of crystallinity.

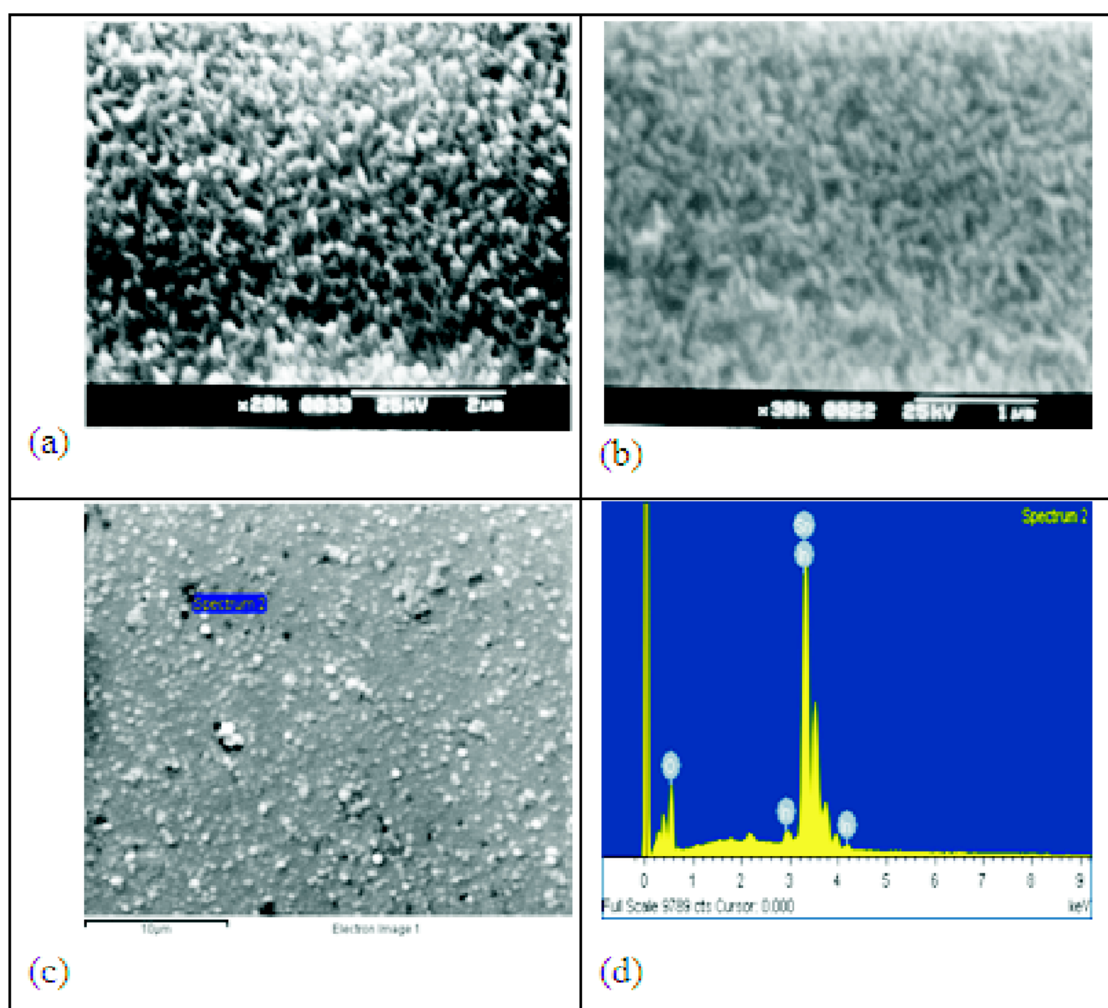

Fig. 4. Scanning Electron Micrograph (SEM) of ITO films deposited under Ar+H_2 ambient with C_H values: (a) 2%, (b) 6%, (c) H-Plasma exposed and (d) EDX spectrum of H-plasma exposed ITO film.

Fig. 4a, b and c show the SEM images of ITO films deposited under $Ar+H_2$ ambient. The SEM image of Ar deposited ITO films is included to make the comparative study of the drastic change of ITO surface morphology. Grains are round in shape for Ar-deposited ITO film whereas elongated grains are formed when the ITO film deposited with C_H = 8%. Elemental analysis has been performed by SEM-EDX attachment to understand the composition of the films, the values has been shown in Table 2 and an energy-dispersive X-ray (EDX) spectrum of hydrogen plasma exposed ITO film (deposited with C_H = 6%) is shown in Fig. 3d. From the result it is clear that with increase of C_H values, there is slight change in O/In ratio that may be the cause of slight decrease of optical transmittance of the ITO film; but significant change in In/Sn ratio is observed that explains the increase of film resistivity as well as the structural diversity.

The 2D and 3D surface topographies and grain distribution profile of as-deposited and hydrogen plasma exposed ITO films, have been studied by Scanning Probe Microscopy to understand the hydrogen effect on surface roughness and surface features shown in Fig. 5. Fig. 5a and Fig. 5b shows the topography of ITO film deposited with Ar ambient whereas Fig. 5c shows the grain size distribution of ITO film deposited under $Ar+H_2$ ambient with C_H = 6%. The comparative study of surface topography (2D and 3D view) of hydrogen plasma exposed ITO films with as-deposited and its grain size distribution are also shown in Fig. 6. The surface roughness of as-deposited and hydrogen plasma ITO films are

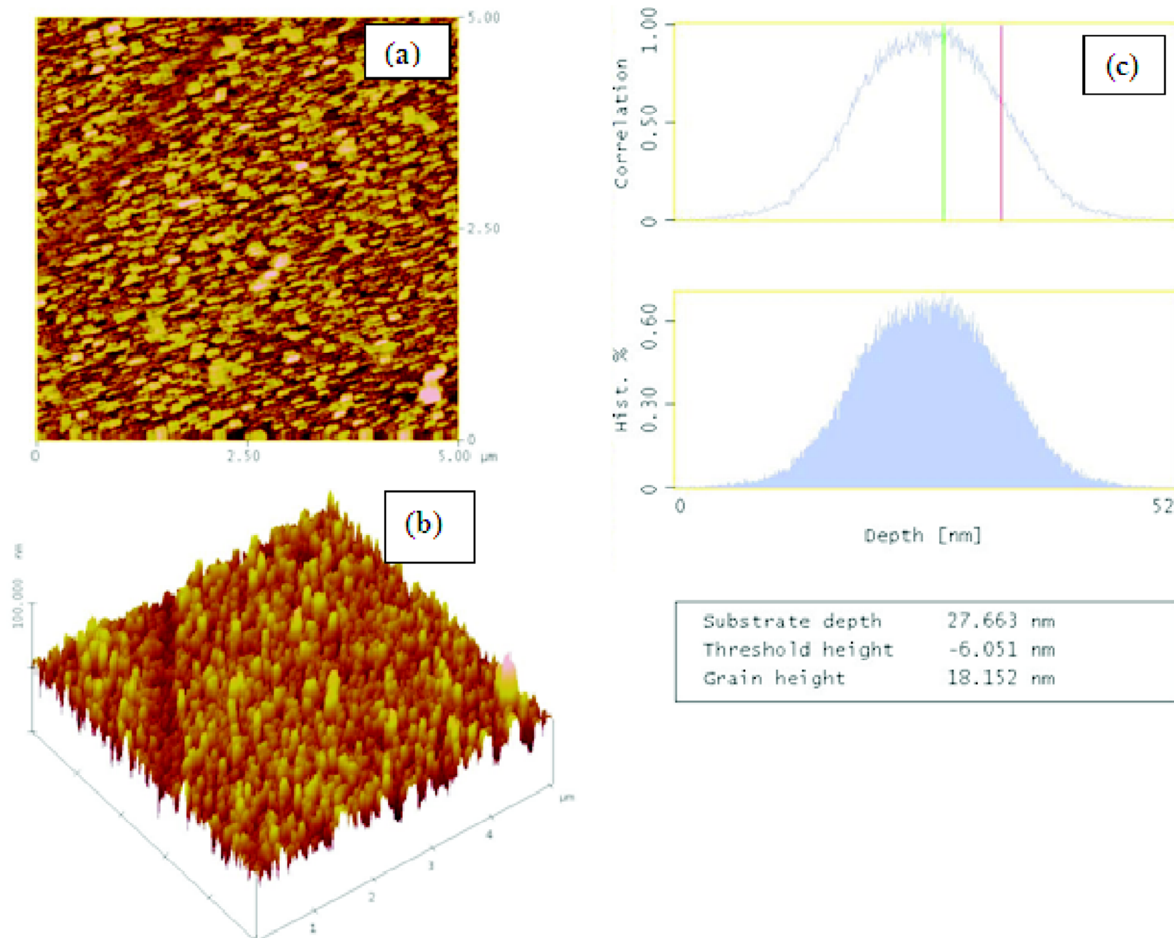

Fig. 5. Atomic Force Microscopy (AFM) image as deposited (C_H=6%) ITO thin film: (a) 2D view, (b) 3D view and (c) corresponding grain distribution profile.

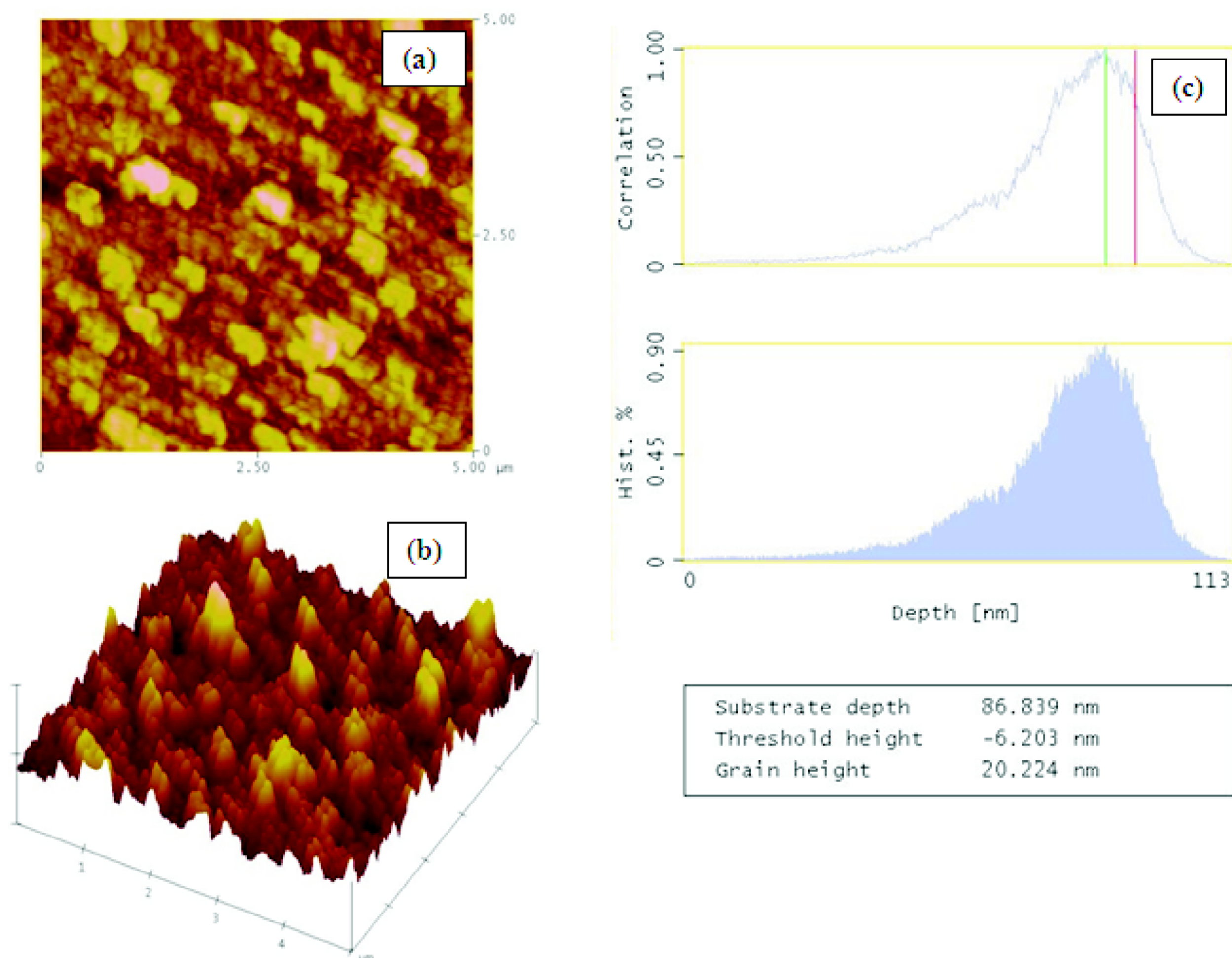

Fig. 6. Atomic Force Microscopy (AFM) image of H-plasma exposed ITO films: (a) 2D view, (b) 3D view and (c) corresponding Grain distribution profile.

7.14 nm and 4.96 nm respectively. We assume that both the high degree of texture and the small roughness of the ITO films are specific properties of films with cubic structure of crystallites[23]. With the increase of C_H values the grain size has increased. Over-higher calcinations temperature (for T ~300°C) enhances the major growth and induces large grains with irregular shapes resulting in a rough surface. But an important observation is that the surface roughness of the $Ar+H_2$ deposited ITO film shows the lower value compared to the Ar deposited ITO film. The grainy character of the surface microstructure with increase of C_H values is decreasing significantly and that is why $Ar+H_2$ deposited ITO surface roughness is less than that of Ar deposited ITO film. Simultaneous hydrogen plasma etching during deposition may be the cause of lower roughness of $Ar+H_2$ deposited ITO film.

Conclusions

Systematic studies on structural, electrical, optical and morphological studies of ITO film due to the effect of H_2 ambient have been done. It has been observed that (222) In_2O_3 crystalline orientation is affected by the H incorporation during deposition and a preferential orientation of the In_2O_3 crystallites in the (400) directions perpendicular to substrate is favored. The intensity of the (400) crystalline peak increases significantly with the increase of C_H value due to reduction of oxygen content in the film. In parallel to the structural change in crystallographic planes, H_2 ambient has sig-

nificant role to change In/Sn composition into ITO films, which initially increases from 11.33 to 11.71 with increases for C_H = 2% value but decreases to 11.098 with further increase of C_H beyond 6%. The variation of In/Sn ratio controls the stoichiometry and may be the cause of the formation of nanocrystallites, void formation in ITO film. This observation suggests that the crystallographic defects process is induced by the hydrogen incorporation with Ar ambient. In parallel to above observations; a dramatic change in the surface morphology as well as surface roughness is observed caused by the H incorporation during deposition. Haze factor of the ITO films also varies with different hydrogen dilution was reported.

Acknowledgement

The authors acknowledge Department of Science and Technology, Govt. of India [DST/TM/SERI/2K10/67(G)] for financial support for pursuing the R&D activity.

References

1. R. Das, K. Adhikary and S. Ray, *Jpn. J. Appl. Phys*., 2008, **47**, 1501.
2. W. J. Jeong, S. K. Kim and G. C. Park, *Thin Solid Films*, 2006, **180**, 506.
3. S. Y. Lien, *Thin Solid Films,* 2010, **518**, S10.
4. B. Parida, H. Y. Ji, G. H. Lim, S. Park and K. Kim, *J. Renew. Sustain. Energy*, 2014, **6**, 053120.
5. E. Gur, S. Tuzemen, B. Kilic and C. Coskun, *J. Phys. Condens. Matter*., 2007, **19**, 196206.
6. J. B. DuBow, D. E. Burkt and J. R. Sites, *Appl. Phys. Lett*., 1976, **29**, 494.
7. M. Nisha, S. Anusha, A. Antony, R. Manoj and M. K. Jayaraj, *Appl. Surf. Sci*., 2005, **252**, 1430.
8. F. E. Akkad, M. Marafi, A. Punnoose and G. Prabu, *Phys. Status Solidi.*, 2000, **177**, 445.
9. Wohlmuth and I. Adesida, *Thin Solid Films*, 2005, **479**, 223.
10. H. Y. Yeom, N. Popovich, E. Chason and D. C. Paine, *Thin Solid Films*, 2002, **411**, 17.
11. H. Morikawa and M. Fujita, *Thin Solid Films*, 2000, **359**, 61.
12. M. Rottmann and K. H. Heckner, *J. Phys. D: Appl. Phys*., 1995, **28**, 1448.
13. Wen Fa Wu and Bishiou Chiou, *Semiconductor. Sci. Technol*., 1996, **11**, 196.
14. K. Itoyama, *Jpn. J. Appl. Phys*., 1978, 17.
15. Tania Konry and Robert S. Marks, *Thin Solid Films*, 2005, **492**, 313.
16. J. H. Hwang, D. D. Edwards, D. R. Kammler and T. O. Mason, *Solid State Ionics*, 2000, **129**, 135.
17. R. Das and H. S. Das, *J. Inst. Eng. India Ser. D*, 2016, **98(2)**, 203.
18. R. Das, H. S. Das, P. K. Nandi and S. Biring, *Appl. Phys. A*, 2018, **124**, 631.
19. R. Das and H. S. Das, *J. Inst. Eng. India Ser. D*, 2017, **98(1)**, 85.
20. K. Jagera and M. Zeman, *Appl. Phys. Lett*., 2009, **95**, 171108.
21. ASTM powder data (ICDD Card 44-1087), 1994.
22. G. K. otcenkov, V. Brinzari, A. Cerneavschi, M. Ivanov, V. Golovanov, A. Cornet, J. Morante, A. Cabot and J. Arbiol, *Thin Solid Films*, 2004, **460**, 315.
23. G. K. otcenkov, A. Cerneavschi, V. Brinzari, A. Cornet, J. Morante, A. Cabot and J. Arbiol, *Sensor. Actuat*., 2002, **B84**, 37.